Acta Pharmaceutica Sinica B 2024;14(9):4045−4058

Chinese Pharmaceutical Association
Institute of Materia Medica, Chinese Academy of Medical Sciences

Acta Pharmaceutica Sinica B

www.elsevier.com/locate/apsb
www.sciencedirect.com

ORIGINAL ARTICLE

Triple three-dimensional MS/MS spectrum facilitates quantitative ginsenosides-targeted sub-metabolome characterization in notoginseng

Ke Zhang [a], Jinru Jia [b], Ting Li [a], Wenjing Liu [c], Pengfei Tu [a], Jian-Bo Wan [d,*], Jun Li [a,*], Yuelin Song [a,*]

[a]*Modern Research Center for Traditional Chinese Medicine, Beijing Research Institute of Chinese Medicine, Beijing University of Chinese Medicine, Beijing 100029, China*
[b]*SCIEX China, Beijing 100015, China*
[c]*School of Pharmacy, Henan University of Chinese Medicine, Zhengzhou 450046, China*
[d]*State Key Laboratory of Quality Research in Chinese Medicine, Institute of Chinese Medical Sciences, University of Macau, Taipa, Macao 999078, China*

Received 7 February 2024; received in revised form 12 April 2024; accepted 22 April 2024

KEY WORDS

Quantitative sub-metabolome characterization;
Ginsenosides;
Structural identification;
Notoginseng;
Full exciting energy ramp-MS^3 spectrum

Abstract Although serving as the workhorse, MS/MS cannot fully satisfy the analytical requirements of quantitative sub-metabolome characterization. Because more information intrinsically correlates to more structural and concentration clues, here, efforts were devoted to comprehensively tracing and deciphering MS/MS behaviors through constructing triple three-dimensional (3×3D)-MS/MS spectrum. Ginsenosides-targeted metabolomics of notoginseng, one of the most famous edible medicinal plants, was employed as a proof-of-concept. Serial authentic ginsenosides were deployed to build the correlations between 3×3D-MS/MS spectra and structure/concentration features. Through assaying ginsenosides with progressive concentrations using QTOF-MS to configure 1st 3D spectrum, the generations of MS^1 spectral signals, particularly multi-charged multimer anions, *e.g.*, $[2M-2H]^{2-}$ and $[2M+2HCOO]^{2-}$ ions, relied on both concentration and the amount of sugar chains. By programming progressive collision energies to the front collision cell of Qtrap-MS device to gain 2nd 3D spectrum, optimal collision energy (OCE) corresponding to the glycosidic bond fission was primarily correlated with the masses of precursor and fragment ions and partially governed by the glycosidation site. The quantitative relationships between OCEs and masses of precursor and fragment ions were utilized to build large-scale quantitative program for ginsenosides. After applying progressive exciting energies to the back collision chamber to build 3rd 3D spectrum, the fragment ion and the decomposition product anion

*Corresponding authors.
E-mail addresses: jbwan@um.edu.mo (Jian-Bo Wan), drlj666@163.com (Jun Li), syltwc2005@bucm.edu.cn (Yuelin Song).
Peer review under the responsibility of Chinese Pharmaceutical Association and Institute of Materia Medica, Chinese Academy of Medical Sciences.

https://doi.org/10.1016/j.apsb.2024.04.029

exhibited identical dissociation trajectories when they shared the same molecular geometry. After ginsenosides-focused quantitative metabolomics, significant differences occurred for sub-metabolome amongst different parts of notoginseng. The differential ginsenosides were confirmatively identified by applying the correlations between 3×3D-MS/MS spectra and structures. Together, 3×3D-MS/MS spectrum covers all MS/MS behaviors and dramatically facilitates sub-metabolome characterization from both quantitative program development and structural identification.

1. Introduction

Because of the potential to bridge non-targeted metabolomics toward targeted metabolomics, chemical homologues-focused metabolomics (also known as sub-metabolomics) serves as an emerging and widely popular term in recent years[1−3]. LC−MS/MS is the most favored analytical tool[4,5], and the qualitative and quantitative performances of MS/MS primarily administrate the sub-metabolomics success. Although MS/MS technologies have experienced rapid developments in terms of both resolution and scan rate[6−8], the analytical requirements of quantitative sub-metabolome characterization cannot be completely addressed, even employing cutting-edge techniques. Primary reasons include that only a portion of MS/MS behaviors of given compounds is recorded by the routine strategies and even worse, less information is taken into account at data processing stage. Here, our attention is paid to pursue a robust pipeline permitting comprehensive MS/MS data acquisition and to explore the correlations of the information against structural and concentration properties.

Following MS/MS spectrum acquisition, those versatile databases, *e.g.*, HMDB[9], Metlin[10], ChemSpider[11,12], and MassBank[13], dramatically facilitate the structural annotation for metabolites-of-interest. However, such high-resolution masses (HR-*m*/*z*)-dependent database retrieval strategy is unable to totally fill the gap from masses to chemical structures because isomers frequently produce identical HR-*m*/*z* lists[14]. When taking relative ion intensity (RII) features into consideration, some auxiliary structural evidences could elevate identification confidences[15,16]. The trajectory of RII against collision energy (CE), termed as breakdown graph[17,18], is inherently governed by the structures and in turn, reflects certain structural properties[18]. Fortunately, an elegant program namely online energy-resolved MS (ER-MS) has been stably developed to acquire breakdown graph for any ion species-of-interest[19]. Due to gathering sigmoid-type breakdown graph of precursor ion residue (usually $[M+H]^+$/$[M-H]^-$) and Gaussian-shaped breakdown graph(s) of all primary fragment ion(s), full CE ramp-MS^2 (FCER-MS^2) spectrum universally implies the dissociation behaviors of the precursor ion against CE. The primary spectral features such as RII_{max}, OCE, and CE_{50}, are termed as the maximum RII of each fragment ion, CE at RII_{max}, and CE at 50% survival rate of precursor ion, accordingly. When incorporating with quantum structural calculation, those features are quantitatively correlated to certain molecular descriptors (MDs), particularly the linkages amongst substructures, leading to a significant growth of structural annotation capacity. If dissociations can be operated in a tandem-in-time manner, for instance 3D ion trap-MS, or when tandem-in-space collision cells are available, *e.g.*, Qtrap-MS equipping two serially coupled collision cells, the follow-up dissociation kinetics of 1^{st}-generation fragment ion will be comprehensively traced *via* operating online ER-MS program for one more time. Similarly, through involving all 2^{nd}-generation breakdown graphs to compose full exciting energy ramp-MS^3 (FEER-MS^3) spectrum[20], quantitative relationships should also exist amongst the spectral features and certain MDs of substructure. Except for molecular formula information, MS^1 spectrum is able to reflect additional structural information because the charge fashion, in particular those multi-charged multimer ions, is also administrated by the structure[21]. Above all, if the aforementioned findings can be fused *via* configuring the triple three-dimensional MS/MS spectrum (3×3D-MS/MS spectrum) that consists of full concentration ramp-MS^1 (1^{st} 3D), FCER-MS^2 (2^{nd} 3D), and FEER-MS^3 (3^{rd} 3D) spectra, the structural identification ability of MS/MS will be significantly advanced.

Although metabolomics is conceptually designed to determine the concentration of every metabolite in given matrices, in practice, MS/MS response, frequently peak area of MS^1 spectral signal[22,23], replaces the concentration role. Though linear correlations occur in theory, such relationships are critically challenged by the insufficient linear dynamic range of the analytical instrument, *e.g.*, QTOF-MS[24]. Except for competitive ionization in the case of numerous co-eluted molecules, the factors dampening linear correlations are largely unknown till now. To address the content-extended distribution styles of metabolites, it should be better to apply multiple-reaction monitoring (MRM) program instead of full scan with QTOF-MS device[25]. The workload thereafter turns to quantitative settings optimization, such as precursor > fragment ion transitions and OCEs, in a high-throughput authentic compound-independent manner. Because ion transitions can be conveniently constructed by pairing precursor and dominant fragment ions, the key to build the monitoring list should be the relationships between OCE and ion masses.

To fulfill the analytical requirements of quantitative sub-metabolome characterization, an attempt is made here to simultaneously improve qualitative and quantitative performances of MS/MS. Regarding qualitative aspect, the fortification of concentration- and energy-resolved programs to conventional MS/MS measurements results in 3×3D-MS/MS spectrum allowing to involve fruitful structural clues. Moreover, concentration-resolved measurements are also programmed to explore the factors suppressing the linear dynamic range, and more importantly, our concerns are also paid to construct MRM program for globally quantitative analysis. Ginsenosides-focused metabolomics of notoginseng is conducted to justify the utility of 3×3D-MS/MS spectrum concept because either ginsenosides or notoginseng have occupied the research hotspot concerning medicinal plants for

decades[26], attributing to the pronounced therapeutical and tonic benefits. The findings are envisioned to profile in depth the distribution styles of ginsenosides in notoginseng, and more importantly, provide a promising analytical pipeline for quantitative sub-metabolome characterization without updating any hardware.

2. Materials and methods

2.1. Chemicals and reagents

Twenty-two dammarane-type ginsenosides (Supporting Information Fig. S1), together with two other ginsenosides, namely Ro (oleanolic acid-type saponin) and F11 (octillol-type saponin), were commercially obtained from Standard Technology Co., Ltd. (Shanghai, China) and Shanghai Yuanye Biotechnology Co., Ltd. (Shanghai, China). The structures of all authentic compounds are depicted in Supporting Information. Eleven saponins owned more than two sugar chains. Nine and thirteen owned protopanaxatriol and protopanaxadiol scaffolds, respectively. Noteworthily, tight structural correlations occurred for certain compounds. For instance, Rd and XVII were a pair of isomers, and F2 (*i.e.,* 20,3-*O*-diglucosyl protopanaxadiol), Rg3 (*i.e.,* 2′-*O*-glucosyl-3-*O*-glucosyl protopanaxadiol), and Rh2 (*i.e.,* 3-*O*-glucosyl protopanaxadiol) served as the step-wise hydrolysis products for Rd (*i.e.,* 2′-*O*-glucosyl-3-*O*-glucosyl-(20-*O*-glucosyl) protopanaxadiol). A natural product namely astragaloside IV was purchased from Standard Technology Co., Ltd. and applied as the internal standard (IS).

Forty-one batches, in total, of different parts of *Panax notoginseng*, comprising sixteen batches of roots (root1−root16), fifteen batches of flowers (flower1−flower15), and ten batches of rhizomes (rhizome1−rhizome10), were collected from the crude material market in Anguo (Hebei, China) and authenticated by one of the authors, Prof. Pengfei Tu. All voucher specimens are deposited in the herbarium of our institute.

LC−MS-grade formic acid, methanol, and acetonitrile (ACN) were purchased from Thermo-Fisher (Pittsburgh, PA, USA). Deionized water (18.2 MΩ cm) was prepared in-house using a Millipore Milli-Q purification apparatus (Bedford, MA, USA).

2.2. Sample preparation

Stock solutions of all ginsenosides were prepared by separately dissolving with methanol or 50% aqueous methanol to appropriate concentrations. An aliquot of each stock solution was pooled to produce the mixed standard solution that subsequently underwent gradual 2-fold dilution using 50% aqueous methanol to yield a panel of calibration samples (Set A). IS was dissolved with 50% aqueous methanol to generate IS solution (20 μg/mL).

After being thoroughly dried and well pulverized, a 1.0 g aliquot of each batch was extracted with 50 mL methanol for 30 min by applying an ultrasonication-assisted manner. Each extract successively underwent 10,000 rpm centrifugation and filtration through a 0.22 μm Nylon membrane to result in an additional set of samples (Set B). Afterwards, 25-fold dilution with methanol was separately conducted for a portion of each extract to yield another series of samples (Set C). Each sample was individually mixed with an equal volume of IS solution to produce all testing samples, 82 in total. All samples belonging to Sets B and C, participated in quantitative sub-metabolomics, aiming to guarantee that all ginsenoside concentrations located within the linear ranges of MRM program. Quality control (QC) sample was yielded by mixing aliquots of all samples in Set B. Progressive 2-fold dilution was carried out for QC sample to give out Set D samples after individually fortifying equal volume of IS solution.

2.3. Biosynthesis of ^{13}C-isotopically labeled Rd

To consolidate the occurrences of multi-charged multimer anions (*e.g.*, $[n\mathrm{M}-n\mathrm{H}]^{n-}$ and $[n\mathrm{M}+n\mathrm{HCOO}]^{n-}$), particularly $[2\mathrm{M}-2\mathrm{H}]^{2-}$ and $[2\mathrm{M}+2\mathrm{HCOO}]^{2-}$, in the apparent $[\mathrm{M}-\mathrm{H}]^{-}$ and $[\mathrm{M}+\mathrm{HCOO}]^{-}$ signals, respectively, ^{13}C-isotopically labeled Rd, as a representative, was biosynthesized from F2 under the catalysis of a UDP-glycosyltransferase namely PgUGT94Q2. The instructions described previously were tightly followed[27]. Briefly, the PgUGT94Q2 gene was cloned into pGEX4T-1 carrier using the primer pair namely PgUGT94Q2-BamHI/PgUGT94Q2-EcoRI and then transmitted into *Escherichia coli* BL21-CodonPlus. *E. coli* harboring the plasmids were cultured to an OD_{600} value of 0.6−0.8 in Luria−Bertani medium fortified with ampicillin at 37 °C. The protein expression was induced by 0.5 mmol/L of isopropyl β-D-thiogalactoside. Cell incubation was conducted at 18 °C for 18 h with continuous 200 rpm oscillation, successively followed by sonication and centrifugation at 8000 rpm at 4 °C for 40 min. Thereafter, the supernatants containing recombinant proteins were responsible to transfer a ^{13}C-isotopically labeled glucosyl moiety from UDP-^{13}C-glucose to C-2′ site of F2 in the reaction buffer. After 12 h-incubation at 35 °C, iced ACN quenched the reaction. Following the removal of protein precipitates, the resultant solution containing the desired product namely ^{13}C-Rd, was subjected onto LC−MS/MS measurements. Moreover, a portion of the solution was combined with appropriate volume of ^{12}C-Rd solution to yield a mixture containing both ^{12}C-Rd and ^{13}C-Rd.

2.4. Configuration of 3×3D-MS/MS spectra for ginsenosides

A given 3×3D-MS/MS spectrum was indeed composed of three apparent 3D spectra, such as full concentration ramp-MS^1 (1^{st} 3D), FCER-MS^2 (2^{nd} 3D), and FEER-MS^3 (3^{rd} 3D) spectra. The mixed standard solution and QC sample took part in all measurements to construct 3×3D-MS/MS spectrum for each ginsenoside, and the biosynthetic samples together with Set A samples merely joined in 1^{st} and 2^{nd} 3D spectral acquisition.

All chromatographic separations were accomplished on Shimadzu LC-20AD_{XR} modular (Kyoto, Japan) through equipping a Waters ACQUITY HSS T3 column (2.1 mm × 100 mm, 1.8 μm, Milford, CT, USA). The elution was undertaken by delivering 0.1% aqueous formic acid (A) and ACN containing 0.1% formic acid (B) in gradient as below: 0−2 min, 15%−37% B; 2−13 min, 37% B; 13−17 min, 37%−40% B; 17−24 min, 40%−95% B; 24−26 min, 95% B; 26−26.1 min, 95%−15% B; 26.1−32 min, 15% B; and total flow rate, 0.2 mL/min. Column oven was maintained at 40 °C and injection volume was 2 μL.

2.4.1. Full concentration ramp-MS^1 spectrum construction

The column outlet was directly linked to ESI interface of QTOF-MS equipment (SCIEX 6600$^+$, Foster City, CA, USA) to record MS^1 spectra for all ginsenosides[28]. Negative ionization polarity was applied and the ion source settings were defined as below: ion source gas 1 (GS1), 50 psi; ion source gas 2 (GS2), 50 psi; curtain gas (CUR), 35 psi; ionspray voltage, −4500 V; temperature, 500 °C; and declustering potential (DP), −60 V. CE for MS^1 experiment was set at −5 eV to avoid in-source collision-induced dissociation (CID), and mass range as 100−3000 Da was

implemented to guarantee the observation of all singly and multiply charged monomer/multimer anions. SCIEX Analyst OS software (Version 2.2) was in charge of data acquisition and processing. Regarding each saponin, MS^1 spectra at different concentration levels were overlaid to produce 1st 3D spectrum.

Moreover, data-dependent acquisition (DDA) algorithm was deployed to automatically trigger MS^2 spectrum recording for the top-10 most abundant ions. CE and CE spread (CES) were set as −40 and 20 eV, respectively, to record all MS^2 spectra. Extensive attention was thereafter paid to assign MS^2 spectral signals to their precursor ions in MS^1 spectra, and the aligned MS^1-MS^2 dataset was thereafter implemented for 2nd 3D spectrum construction and structural annotation as well.

2.4.2. *FCER-MS^2 spectrum construction*

The protocols described previously were deployed to build FCER-MS^2 spectrum[19]. The column outlet was linked to Qtrap-MS device (SCIEX 5500, Foster City, CA, USA) and negative ionization polarity was also applied. SCIEX Analyst software (Version 1.6.3) administrated spectrum recording and data processing. Noteworthily, compared to either $[M-H]^-$ or $[M+2HCOO]^{2-}$, $[M+HCOO]^-$ ion was more frequently selected to produce fragment ions due to the greater abundances. All breakdown graph regression as well as key features (*e.g.*, CE_{50}, OCE, and RII_{max}) calculation was accomplished by GraphPad Prism 7.0 software (San Diego, CA, USA).

Further, all CE_{50} values calculated from sigmoid-shaped breakdown graphs were concerned to explore the linear correlations with masses of precursor ions using GraphPad Prism 7.0 software. OCEs from all Gaussian-shaped breakdown graphs were used to pursue the correlations with masses of both precursor and fragment ions through surface fitting with OriginPro 9 software (Northampton, MA, USA).

2.4.3. *FEER-MS^3 spectrum measurements*

Qtrap-MS was also implemented to build FEER-MS^3 spectra. The 1st-generation fragment ions resulted from neutral cleavage of the glycosyl residue(s), such as the aglycone anions (*e.g.*, *m/z* 475.4 and 459.4) and other ions-of-interest were allowed to undergo the follow-up CID in LIT chamber for the sake of FEER-MS^3 spectrum measurements. Sigmoid-shaped or multiply iterative breakdown graphs were obtained for MS^3 spectral signals through programming progressive EE levels[20]. Each FEER-MS^3 spectrum was constructed *via* assembling those breakdown graphs after appropriate normalization. The primary descriptors, such as EE_{50}, RII_{OEE}, and OEE that were termed as EE at 50% survival rate of 1st-generation fragment ion, the maximum RII of each 2nd-generation fragment ion, and EE at RII_{OEE}, respectively, were calculated from regressive equations. Because a single 1st-generation fragment ion exactly corresponded to one FEER-MS^3 spectrum, a single ginsenoside usually possessed more than one FEER-MS^3 spectra.

Noteworthily, when Q1 and q2 units merely operated functions to guide ion beam entering LIT chamber, the resultant spectrum was termed as FEER-MS^2 because $[M-H]^-$ ion rather than 1st-generation fragment ion received CID in LIT cell. FEER-MS^2 spectra were built for all authentic ginsenosides as well as those differential variables. A single compound merely owned one FEER-MS^2 spectrum. Obviously, FEER-MS^2 spectrum was acquired by LIT whilst FCER-MS^2 spectrum was recorded using q2 cell. All EE_{50} values and OEEs calculated from sigmoid-shaped and multi-iterative breakdown graphs, respectively, were utilized to explore the correlations with masses of 1st- and 2nd-generation fragment ions.

2.5. *Quantitative comparison of ginsenosides-focused sub-metabolome*

MS^1-MS^2 dataset of QC sample was carefully interpreted, and those well-defined mass fragmentation laws were adopted to decipher each MS^1-MS^2 item to putative identities[26]. The linear correlations between OCEs and the masses of precursor and fragment ions were applied to calculate OCEs for all 95 detected ginsenosides. Afterwards, the information composed MRM list for the quantitative characterization of all annotated ginsenosides and IS in both Sets B and C samples. QC sample was assayed after every four analytical runs. Set D samples were utilized as the so-called diluted universal metabolome standard (UMS) solutions for method validation by following the instructions described previously[20]. Analyst OS software was responsible for quantitative data processing.

Peak area ratio dataset of all testing samples together with those QC samples was outputted as a ".csv" file. Because each sample generated a column with constant length, data alignment wasn't mandatory actually. Principal component analysis (PCA) was undertaken by SIMCA-P 14.0 software (Umetrics, Umeå, Sweden) after that all variables were Pareto-scaled.

3. Results and discussions

3.1. *Correlations between 3×3D-MS/MS spectra and ginsenoside structures*

3.1.1. *Correlations between 1st 3D spectrum and concentration/structure*

After correlating full concentration ramp-MS^1 spectra of all authentic saponins with their structure and concentration properties, our findings included:

1) Multicharged (multimer) anions were widely detected for ginsenosides. In MS^1 spectrum of F2 (Fig. 1A), as a representative, the primary signals at *m/z* 783.4912, 806.4941, 829.4990, 1198.7422, 1221.7483, 1614.0029, 2006.2521, and 2398.5050, were deciphered as $[M-H]^-$, $[2M+HCOO-H]^{2-}$, $[M+HCOO]^-$ (containing $[2M+2HCOO]^{2-}$), $[3M+HCOO-H]^{2-}$, $[3M+2HCOO]^{2-}$, $[2M+HCOO]^-$ (containing $[4M+2HCOO]^{2-}$), $[5M+2HCOO]^{2-}$, and $[3M+HCOO]^-$ (containing $[6M+2HCOO]^{2-}$), respectively. Such multicharged (multimer) anions were also found in MS^1 spectra of F2 isomers, *i.e.*, Rg3 (Fig. 1B) and LXXV (Fig. 1C).
2) $[2M-2H]^{2-}$ or $[2M+2HCOO]^{2-}$, the occurrence of which could be indicated by the signal at 0.5 Da greater than monoisotopic signal for $[M-H]^-$ or $[M+HCOO]^-$, was eligible to differentiate monodesmosidic and bidesmosidic saponins. When comparing MS^1 spectra among isomers, *e.g.*, F2, Rg3, and LXXV (Fig. 1), an obvious signal at *m/z* 829.9978 merely occurred for F2 instead of either Rg3 or LXXV, and was interpreted as $[^{12}C-F2+^{13}C-F2+2HCOO]^{2-}$. To justify such speculation, spectrum matching was conducted between ^{12}C-Rd and the mixture of ^{13}C-Rd and ^{12}C-Rd, and the significant abundance of *m/z* 992.0549 ($[^{12}C\text{-Rd}+^{13}C\text{-Rd}+2HCOO]^{2-}$) provided solid evidence (Supporting Information Fig. S2). When incorporating other MS^1 spectra, the signal at 0.5 Da

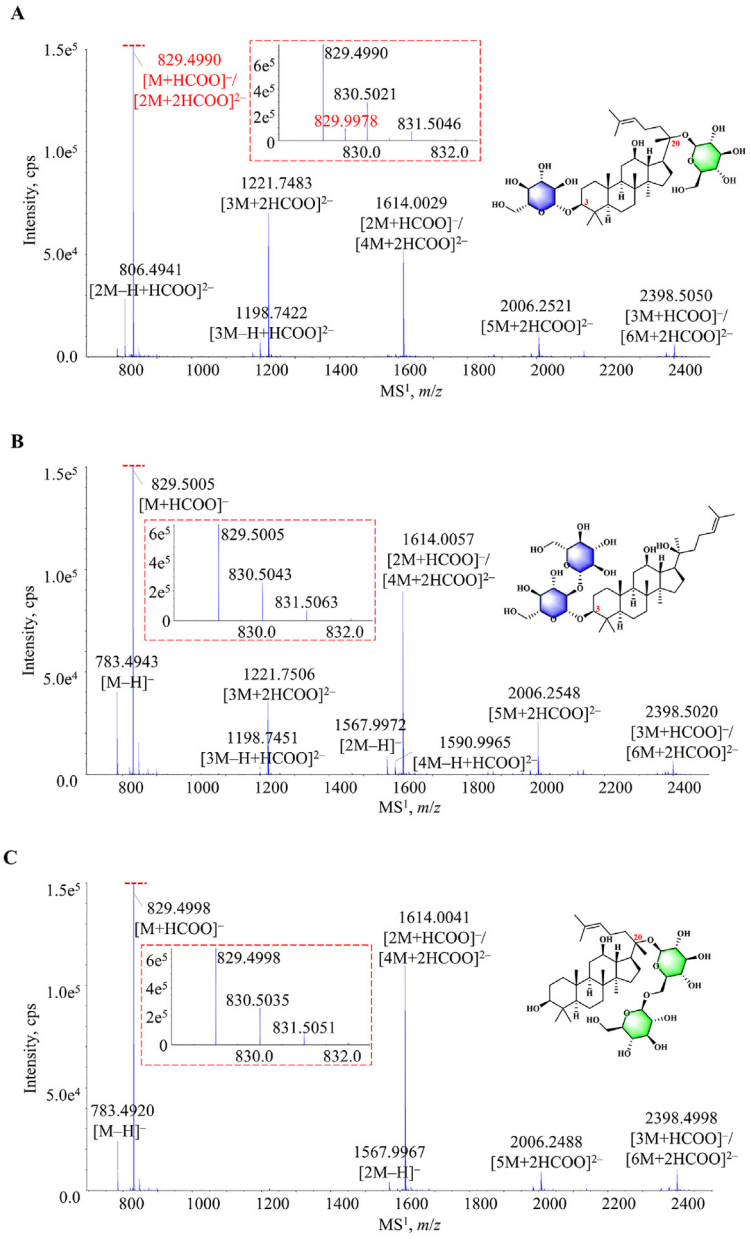

Figure 1 MS^1 spectra for F2 (A), Rg3 (B), and LXXV (C). Range of *m/z* 828−833 is zoomed to highlight the difference, and the primary signals are assigned.

greater than monoisotopic quasi-molecular ion was a unique feature for bidesmosidic ginsenosides.

3) Being different from the classical isotopic rule[29], the presence of such multi-charged multimer anions reduced the abundance ratio between the apparent monoisotopic $[M-H]^-$ (or $[M+HCOO]^-$) ion and ^{13}C-isotopic one, termed as $ISR_{1:0}$ [30], when comparing bidesmosidic and monodesmosidic ginsenoside isomers (Supporting Information Fig. S3). For instance, at the relative high concentrations, $ISR_{1:0}$ values of F2 and Rg1 were approximately 0.38, accordingly, dramatically lower than their monodesmosidic isomers (about 0.40) such as Rg3, LXXV, and Rg2, as well as F11 and Rf.
4) Chromatographic co-elution widely occurred when measuring notoginseng extract. A variety of hetero-multimer anions were visible when the co-elution of saponins[31], *e.g.*, $[M_1+M_2+HCOO]^-$ and $[M_1+M_2+2HCOO]^{2-}$. MS^1 spectrum for the co-elution of Re and Rg1 is shown in Supporting Information Fig. S4, and *m/z* 918.5237, 1318.7721, 1391.8014, 1719.0211, and 1792.0494 existed as hetero-multimer anions.
5) The abundances of primary signals relied on both concentration and the amount of sugar chains, and the linear range less than three orders of magnitude occurred for $[M+HCOO]^-$ of each saponin. The linear range of the peak area of each primary signal against concentration level for bidesmosidic ginsenoside, F2 for instance (Fig. 2A) was moderately narrower than that of monodesmosidic isomer, *e.g.*, Rg3 or LXXV (Supporting Information Fig. S5A and S5B). Further, the abundance ratio of the apparent monoisotopic $[M-H]^-$ (or $[M+HCOO]^-$) against the one with +0.5 Da distance, namely

$ISR_{0.5:0}$ [30], was proportional to the logarithmic concentration, indicating that $ISR_{0.5:0}$ also exhibited a concentration-dependent manner (Supporting Information Fig. S6).

6) The involvement of all primary signals was able to gently boost the linear correlation of peak area against concentration. Particularly, the summed peak areas of all relevant signals resulted in slightly greater increment for the upper limit of quantification of Rg3 or LXXV (Fig. S5C and S5D) when comparing with F2 (Fig. 2B).

Above all, MS^1 spectrum was jointly governed by structure, concentration, and chromatographic purity, and implied vital structural information. Limited linear dynamic range existed for each signal, even the summed peak area, and it was thereby extremely important to develop MRM program for quantitative sub-metabolomics.

3.1.2. *Relationships between FCER-MS^2 spectrum and structure*

After paying extensive attention to FCER-MS^2 spectrum that was built by assembling the breakdown graphs of primary signals in MS^2 spectrum, the primary parameters such as CE_{50}, OCE, and RII_{max} of all authentic ginsenosides are illustrated in Supporting Information Table S1. Except for the correlations proposed previously[19,32], the other findings included:

1) Different FCER-MS^2 spectra frequently appeared within isomers, though they usually shared identical masses for fragment ions, *e.g.*, F2, Rg3, and LXXV (Fig. 3). However, 20*S*- and 20*R*-configurational isomers, *e.g.*, 20*S*-protopanaxatriol *vs.* 20*R*-protopanaxatriol (Supporting Information Fig. S7), shared the totally same FCER-MS^2 spectra because all differences were distributed within the empirical tolerances as ±0.5 eV, ±0.5 eV, and 10% for CE_{50}, OCE, and RII_{max}, accordingly.
2) Because greater molecular weight intrinsically corresponded to higher degree of freedom[33], positive correlations roughly existed for absolute values of CE_{50} against masses of $[M-H]^-$ ions (Supporting Information Fig. S8). However, different CE_{50} values usually occurred crossing positional isomers (Fig. 3), *e.g.*, F2 (−28.24 eV), Rg3 (−35.77 eV), and LXXV (−31.25 eV).
3) The absolute value of OCE (|OCE|) corresponding to the neutral loss of sugar residue(s) from $[M-H]^-$, $[M+HCOO]^-$, or $[M+2HCOO]^{2-}$ was positively and conversely correlated with the masses of precursor and fragment ions, respectively. After taking OCEs from all authentic saponins into account, the regressive equation came out as $z = -14.42424 - 0.06878x + 0.03519y$ ($R^2 = 0.8416$), where z is OCE of the concerned fragment ion, x is precursor ion mass, and y is fragment ion mass (Fig. 4).
4) OCE was also a function of glycosidation site. When comparing FCER-MS^2 spectra amongst F2, Rg3, and LXXV, different OCEs were observed for *m/z* 621.4 (−34.79 eV, −44.79 eV, and −35.42 eV, Fig. 3), corresponding to glucosyl residue cleavages from C-20, C-2′, and C-6′ sites, respectively. After comparing several isomers, *e.g.*, Rh2 *vs.* CK, Rh1 *vs.* F1, Rg1 *vs.* Rf, and Rd *vs.* XVII, the expelling of C-20 sugar residue required lower |OCE| than the other sites.
5) The greatest RII_{max} frequently occurred for the fragment ions resulting from the loss of a single sugar residue. However, sugar residue anions, such as *m/z* 131.0 ($[pentosyl-H]^-$), 149.0 ($[pentosyl+H_2O-H]^-$), 161.0 ($[hexosyl-H]^-$), 179.1 ($[hexosyl+H_2O-H]^-$), 191.1 ($[hexosyl+pentosyl+H_2O-C_4H_8O_4-H]^-$), 221.1 ($[2\times hexosyl+H_2O-C_4H_8O_4-H]^-$), 251.1 ($[2\times hexosyl+H_2O-C_3H_6O_3-H]^-$), 323.1 ($[2\times hexosyl-H]^-$), and 341.1 ($[2\times hexosyl+H_2O-H]^-$), possessed greater RII_{max}, when most, even all glycosyl groups linked to C-20 site. As shown in Fig. 3, RII_{max} of *m/z* 621.4 serves as the greatest value for F2 or Rg3. FCER-MS^2 spectrum of LXXV (Fig. 3C, Table S1) gave out greater RII_{max} for *m/z* 179.1 (100%), 323.1 (71.07%), 221.1 (35.61%), and 161.0 (27.59%) than *m/z* 621.4 (13.64%), 459.4 (7.84%), and 375.3 (3.84%). Such phenomenon was also observed for FCER-MS^2 spectra comparison between Rd and XVII (Supporting Information Fig. S9).

Consequently, FCER-MS^2 spectrum covered all dissociation trajectories of quasi-molecular ion, and in turn, the information mainly reflected the linkage properties among the substructures. Noteworthily, the correlations between OCE and masses of both precursor and fragment ions facilitated quantitative MRM program development.

3.1.3. *Correlations between FEER-MS^3 spectrum and substructure*

The parameters for FEER-MS^3 spectra of selected 1st-generation fragment ions, such as EE_{50}, OEE, RII_{OEE}, are summarized in Supporting Information Table S2. After paying attention to FEER-MS^3 spectra that comprised sigmoid-shaped and multiply iterative breakdown graphs of MS^3 spectral signals, the correlations with substructures included:

1) Great fitting occurred for multiple iterative curve towards the trajectory of 2nd-generation fragment ion abundance against EE, while sigmoid curve well fitted the breakdown graph of residual 1st-gengeration fragment ion. Taking FEER-MS^3 spectrum of *m/z* 799.5 ($[Re-H-Rha]^-$, Fig. 5F) as a representative, 2nd-generation fragment ions such as *m/z* 161.0, 179.1, 475.4, 619.4, and 637.4 were assigned with multiple iterative curves, whereas *m/z* 799.5 produced sigmoid-shaped curve.
2) Similar to the laws observed for FCER-MS^2 spectrum, absolute values of EE_{50} were positively correlated with 1st-fragment ion masses, and OEE corresponding to the sugar residue cleavages was collectively governed by masses of 1st- and 2nd-generation fragment ions together with dissociation site (Supporting Information Fig. S10).
3) FEER-MS^3 spectrum of certain 1st-gengeration fragment ion for a given ginsenoside was completely consistent with FEER-MS^2 spectrum of the hydrolysis product anion when they shared the same molecular geometries (Table S2). Re as a case (Fig. 5A), 1st-generation fragment ions in MS^2 spectrum were assigned (Fig. 5B), and FEER-MS^3 spectra were built for 1st-generation fragment ions generated by glycosyl residue cleavages. After applying the empirical tolerances as ±0.005 V, ±0.005 V, and 10% for EE_{50}, OEE, and RII_{OEE}, respectively, FEER-MS^3 spectra of *m/z* 475.4, 637.4, 783.5, and 799.5 for Re agreed well with FEER-MS^2 spectra of its progressive hydrolysis product anions (Fig. 5C–F), such as protopanaxatriol, Rh1 (*i.e.,* 6-*O*-Glc protopanaxatriol), Rg2 (*i.e.,* 2′-*O*-Rha-6-*O*-Glc protopanaxatriol), and Rg1 (*i.e.,* 20,6-*O*-*di*Glc protopanaxatriol). FEER-MS^3 spectrum of *m/z* 637.4 for Rg1 or Rg2 was fully consistent with FEER-MS^2 spectrum of the decomposition product (*i.e.,* Rh1) anion. Moreover, Rg1, Rg2, and Rh1 shared identical FEER-MS^3 spectrum of *m/z* 475.4, which was also the same as FEER-MS^2 spectrum of protopanaxatriol anion.

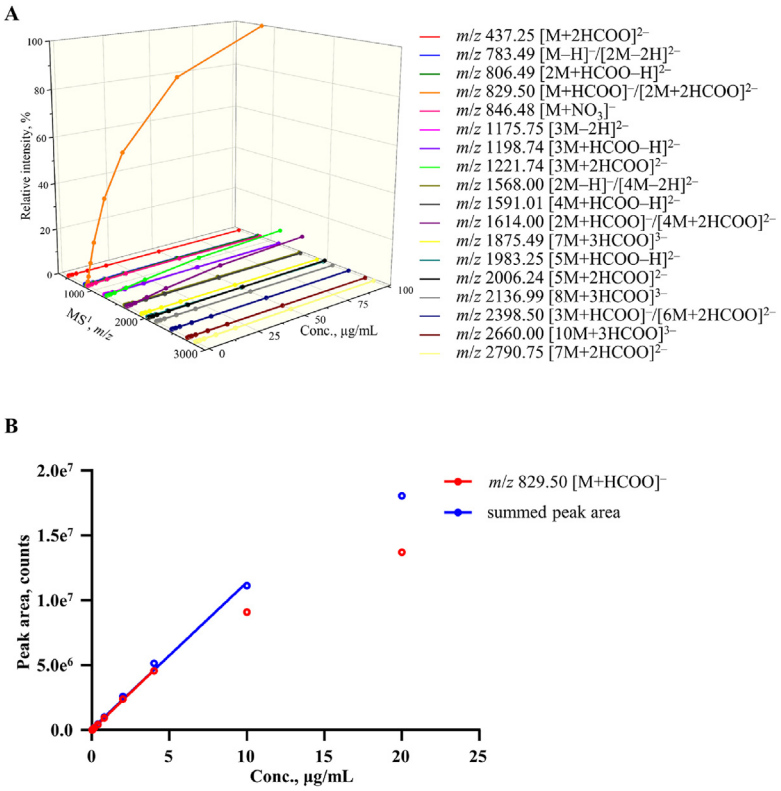

Figure 2 Full concentration ramp-MS[1] spectrum (A) and the summed peak area of all primary signals or the most abundant signal (*i.e., m/z* 829.50 $[M+HCOO]^-$) against concentration profile (B) of F2.

4) FEER-MS[3] of a given ginsenoside was different from FEER-MS[2] belonging to the hydrolysis product isomer. Similarly, when two saponins owned isomeric substructure, different FEER-MS[3] usually occurred for the fragment ions although possessing the same *m/z* profiles. Representatively, FEER-MS[3] spectra of *m/z* 637.4 and 799.5 for Re were significantly different from FEER-MS[2] of F1 (*i.e.,* 20-*O*-Glc protopanaxatriol, Fig. 5D) and Rf (*i.e.,* 2′-*O*-Glc-6-*O*-Glc protopanaxatriol, Fig. 5F). FEER-MS[3] of *m/z* 637.4 for either Rg1 or Rg2 was different from FEER-MS[2] of F1 anion. Differences appeared for FEER-MS[3] of *m/z* 621.4 when comparing Rg3 and LXXV.

FEER-MS[3] spectrum globally covered the dissociation trajectories from the chosen 1st-generation fragment ion to 2nd-generation fragment ions, thus implying the substructure properties. More importantly, the matching between FEER-MS[3] of certain 1st-generation fragment ion for compound-of-interest and FEER-MS[2] of appropriate decomposition product anion facilitated definite substructure identification.

Obviously, 3×3D-MS/MS spectra included all MS/MS behaviors of a given ginsenoside. To achieve confirmatively structural identification of ginsenosides, HR-MS/MS masses were firstly converted to elemental compositions, and afterwards, 1st, 2nd, and 3rd 3D-MS/MS spectra were applied to provide skeleton, the amount of sugar chain, linkage information amongst substructures, and the characteristics of substructures, leading to a promising "top-down" structural annotation strategy[34] where the fragment ions were successively identified *via* matching with serial suspected compounds and linked by utilizing OCE features.

3.2. *Ginsenosides-focused qualitative analysis of QC sample*

The 1st-generation fragment ions were carefully assigned to their precursor ions to produce a MS[1]-MS[2] dataset. Inquiry of each MS[1]-MS[2] item to the well-constructed data libraries[26,35–37] was conducted to reach plausibly structural annotation for ginsenosides in QC sample. Noteworthily, when assigning MS[2] spectral signals of ^{13}C-Rd, the abundance of *m/z* 784.4962 was dramatically greater than *m/z* 783.4925 (Supporting Information Fig. S11A), indicating that ^{12}C-glycosyl residue cleavage at C-20 site dominated the initial fragmentation pathway rather than ^{13}C-glycosyl moiety at C-2'. Referring to the chemical structure, the mass cracking channels in response to the primary MS[2] signals of ^{13}C-Rd are proposed in Fig. S11B. This finding integrating those well-proposed patterns[36,37] was applied to decipher each MS[1]-MS[2] item to plausible identities, after that HR-masses were converted to elemental compositions. Consequently, 95 ginsenosides (Supporting Information Table S3) were found and putatively characterized, and eighteen identities (marked with $^{\Delta}$ symbol) were consolidated by authentic compounds.

3.3. *Quantitative ginsenosides-targeted sub-metabolome comparison amongst different notoginseng parts*

As aforementioned, the fragment ions yielded by dissociating a single sugar residue from $[M+HCOO]^-$ usually served as the most abundant species, and ion transition as $[M+HCOO]^-$ > [M−H−glycosyl residue]$^-$, *e.g.*, *m/z* 991.5 > 783.5 for Rd, was thereby implemented for quantitative analysis in most cases. $[M-H]^-$ > $[M-H-malonyl-H_2O]^-$, *e.g.*,

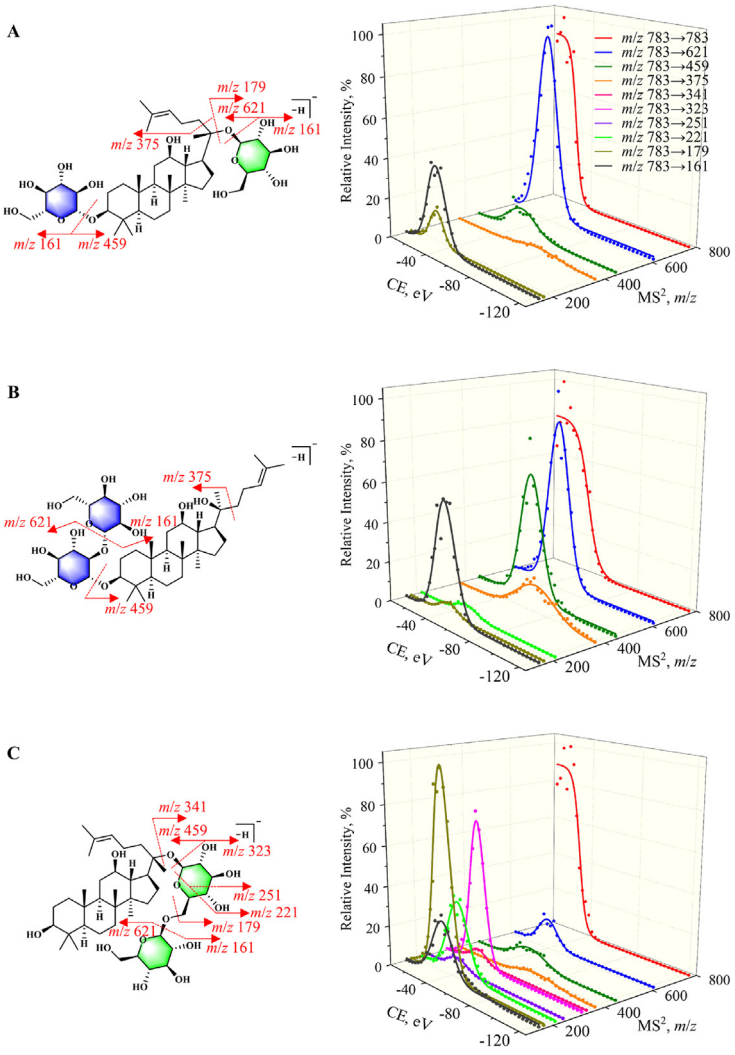

Figure 3 FCER-MS^2 spectra of $[M-H]^-$ for F2 (A), Rg3 (B), and LXXV (C), through assembling sigmoid-shaped breakdown graphs of *m/z* 783.5, and Gaussian-shaped breakdown graphs of *m/z* 621.4, 459.4, 375.3, 341.1, 323.1, 251.1, 221.1, 179.1, and 161.0. The mass fragmentation pathways being responsible for those fragment ions are proposed.

m/z 885.5 > 781.5, were employed for malonyl-ginsenosides, *e.g.*, compound **18**[38]. Thereafter, the relationships between OCE and the masses of precursor and fragment ions were applied to calculate CE settings for all 95 detected ginsenosides. Ultimately, MRM measurement list is programmed as Table S3, and the representative chromatogram is exhibited in Supporting Information Fig. S12.

Set D samples participated in method validation assays in terms of linearity, sensitivity, intra- and inter-day variation, and repeatability. The results of all assays are summarized in Table S3. Fortunately, the developed LC−MRM program was reliable for the quantitative characterization of ginsenosides-focused sub-metabolome.

Regarding those ginsenosides with inferior contents (labeled with * symbol, Table S3), the peak area ratios obtained from Set B samples were directly imported into the quantitative dataset. For the abundant ginsenosides (labeled with # symbol, Table S3), the peak area ratios from Set C samples were multiplied by 25 prior to entering the dataset. After involving QC samples, the dataset was subjected to PCA treatment. The first two principal components accounted for a total of 95.03% variables (91.4% for PC1 and 3.63% for PC2). The score scattering plot and the loading plot are shown in Fig. 6A and B, respectively. The dots corresponding to QC sample tightly gathered around the origin (Fig. 6A), suggesting that the developed quantitative program was reliable. All batches were roughly divided into three clusters, exactly referring to the different parts (Fig. 6A). Regarding the loading plot, dots tagging **14**, **16**, **17**, **32**, **35**, **36**, **40**, **42**, **43**, **45**, **47**, **49**, **50**, **53**, **59**, **60**, **68**, and **78** (Fig. 6B and Table S3), eighteen ones in total, were the primary contributors to the grouping fashion. Accumulation of **14**, **16**, **17**, **32**, **40**, **43**, **45**, **47**, **53**, and **68** occurred in the roots and rhizomes, whereas the flowers contained abundant **35**, **36**, **42**, **49**, **50**, **59**, **60**, and **78**. Thereof, ten variables (**14**, **16**, **17**, **40**, **45**, **50**, **53**, **59**, **60**, and **68**) were unambiguously identified *via* matching with authentic compounds. The summarized relationships were thereafter applied for confidence-enhanced identification of the others.

Taking an isomer set consisting of **32**, **36**, and **43** as the representatives, the roots and rhizomes contained abundant **32** and **43**, whereas the flowers were rich in **36**. The inquiry of MS^1-MS^2

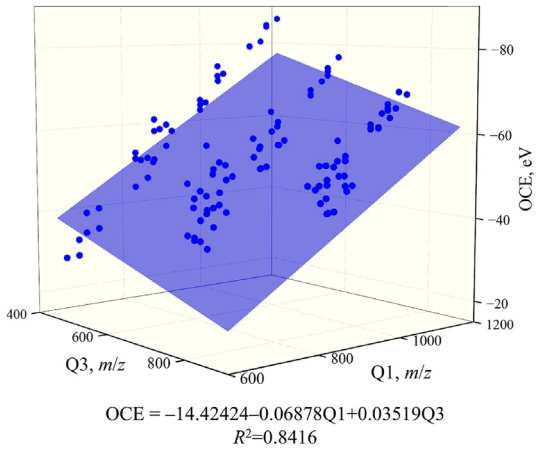

Figure 4 The correlations (R^2 = 0.8416) of optimal collision energy (OCE, *z*-coordinate) against the masses of precursor (Q1, *x*-coordinate) and fragment ions (Q3, *y*-coordinate).

items to the data library outputted plausible identities as notoginsenoside R4 and isomers ($C_{59}H_{100}O_{27}$). The presences of *m/z* 619.3166, 642.3204, 665.3254, 1240.1434, and 1286.1543 in every 1st 3D spectrum, were characterized as $[M-2H]^{2-}$, $[M-H+HCOO]^{2-}$, $[M+2HCOO]^{2-}$, $[^{13}C\text{-}M+M-2H]^{2-}$, and $[^{13}C\text{-}M+M+2HCOO]^{2-}$, respectively, indicating each isomer owned two sugar chains. The prominent 1st-generation fragment ions, such as *m/z* 1107.5952 ($[M-H-pentosyl]^-$), 1077.5867 ($[M-H-hexosyl]^-$), 945.5407 ($[M-H-pentosyl-hexosyl]^-$), 783.4912 ($[M-H-pentosyl-2\times hexosyl]^-$), 621.4339 ($[M-H-pentosyl-3\times hexosyl]^-$), 459.3882 ($[M-H-pentosyl-4\times hexosyl]^-$), 323.0950 ($[2\times hexosyl-H]^-$), 221.0656 ($[hexosyl+C_2H_4O_2-H]^-$), 191.0544 ($[pentosyl+C_2H_4O_2-H]^-$), 179.0577 ($[hexosyl+H_2O-H]^-$), 161.0447 ($[hexosyl-H]^-$), 149.0410 ($[pentosyl+H_2O-H]^-$), and 131.0322 ($[pentosyl-H]^-$) disclosed the building blocks such as four hexosyl groups (always glucosyl), one pentosyl (*e.g.*, arabinosyl or xylosyl), and one protopanoxadiol scaffold, and hexosyl and pentosyl severed as the outer moieties for the two sugar chains. Moreover, *m/z* 353.1085 ($[pentosyl+hexosyl+C_2H_4O_2-H]^-$), corresponding to the cross-ring fission of hexosyl moiety, appeared for **32** and **43**, instead of **36**, suggesting a pentosyl→hexosyl→hexosyl axis for **32** and **43**. Referring to 2nd 3D spectra, comparable OCE features of *m/z* 1107.5952 (−39.55 *vs.* −39.22 eV) and 1077.5867 (−32.90 *vs.* −33.79 eV) occurred between **32** and **43**, and either was different from −38.54 and −31.28 eV of **36** (Supporting Information Table S4), indicating greater structural similarity between **32** and **43**. Afterwards, attention was forwarded to matching 3rd 3D spectra that were generated by 1st-generation fragment ions

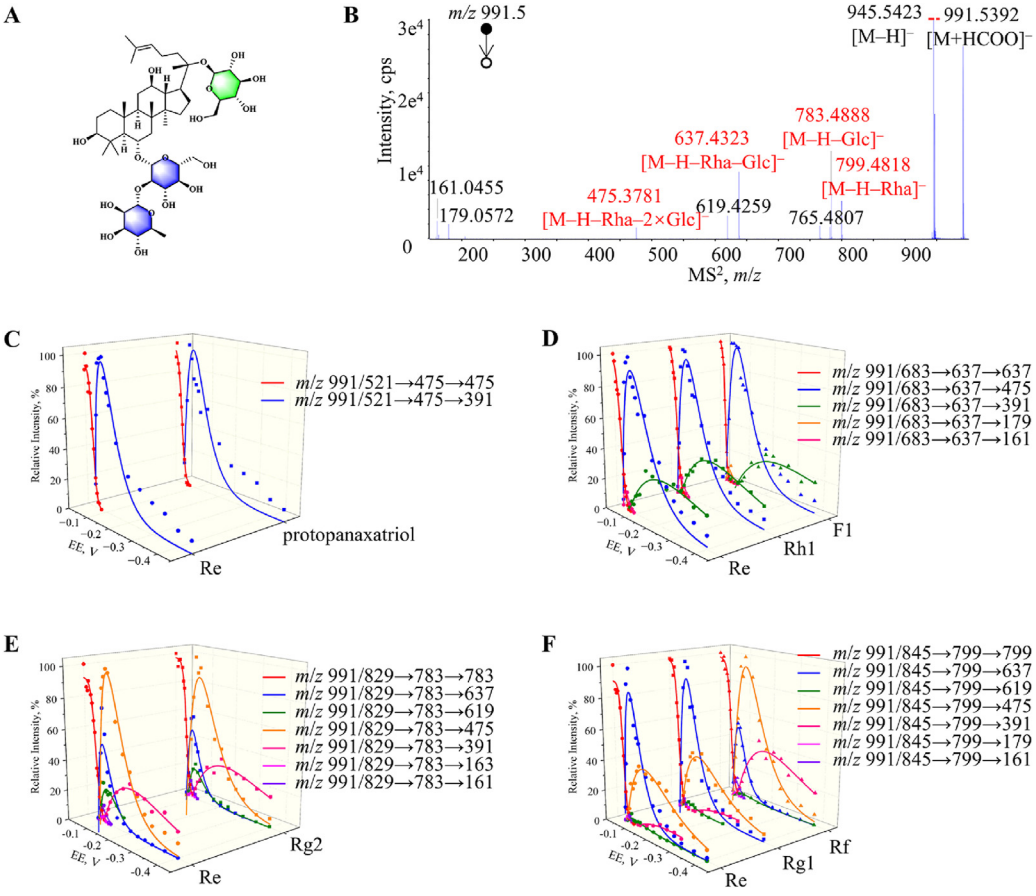

Figure 5 FEER-MS^n spectra (n = 3 for Re and n = 2 for the other compounds) comparison between the concerned fragment ions of Re and anions of suspected decomposition products. Structure (A) and MS^2 spectrum (B) of Re, FEER-MS^n spectra of *m/z* 475.4 for Re and protopanoxatriol (C), FEER-MS^n spectra of *m/z* 637.4 for Re, Rh1, and F1 (D), FEER-MS^n spectra of *m/z* 783.5 for Re and Rg2 (E), and FEER-MS^n spectra of *m/z* 799.5 for Re, Rg1, and Rf (F).

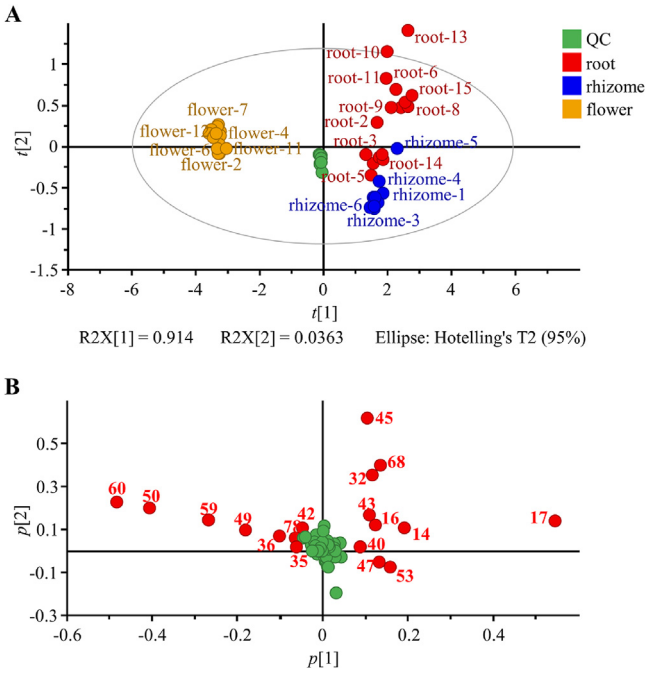

Figure 6 Score scattering plot (A) and loading plot (B) after principal component analysis of the quantitative ginsenoside-focused sub-metabolome for different parts of notoginseng.

corresponding to sequentially expelling sugar residues, with FEER-MS^2 spectra of authentic compounds that were the potential hydrolysis products. FEER-MS^3 spectra of *m/z* 945.5, 783.5, 621.4, and 459.4 for **32**, **36**, or **43** were identical with FEER-MS^2 spectra of serial homologous compounds namely Rd (*i.e.,* 20-*O*-Glc-Rg3), Rg3 (*i.e.,* 3-*O*-Glc(1→2)-Rh2), Rh2 (*i.e.,* 3-*O*-Glc-protopanaxadiol), and protopanaxadiol anions, respectively (Fig. 7A−D), and nonetheless, different from those of XVII (20-*O*-Glc-(1→2)-F2), F2/LXXV (*i.e.,* 3-*O*-Glc-CK/20-*O*-Glc-(1→2)-CK), and CK (*i.e.,* 3-*O*-Glc-protopanaxadiol). FEER-MS^3 spectra of *m/z* 1077.6 ([M−H−hexosyl]$^-$) for **32**, **36**, and **43** were different from FEER-MS^2 spectra of Rc (*i.e.,* 20-*O*-Ara$_f$-(1→6)-Rd), Rb2 (*i.e.,* 20-*O*-Ara$_p$-(1→6)-Rd), and Rb3 (*i.e.,* 20-*O*-Xyl-(1→6)-Rd) (Fig. 7E). In addition to *m/z* 945.5, the sugar residue anions at *m/z* 455.1 ([2×hexosyl+pentosyl−H]$^-$), 353.1, 323.1, and 311.1 exhibited great RII$_{OEE}$ values in FEER-MS^3 spectra of *m/z* 1077.6 when assaying **32** and **43** (Fig. 7E and Table S4). Because different fragment ion abundance resulted from sugar substitution at C-3/6 and C-20, the pentosyl→hexosyl→hexosyl axis should exist at C-20 site of either **32** or **43**. On the other side, 2nd-generation fragment ions corresponding to sequential glycosyl residue cleavages, such as *m/z* 945.5, 915.5, 783.5, 765.5, 621.4, and 459.4, exhibited great RII$_{OEE}$ features for **36**, suggesting that more glycosyl groups located at C-3 site (Fig. 7E and Table S4). FEER-MS^3 spectrum of *m/z* 1107.6 ([M−H−pentosyl]$^-$) for **32** or **36** was identical with FEER-MS^2 spectrum of deprotonated Rb1 (*i.e.* 20-*O*-Glc-(1→6)-Rd, Fig. 7F), whilst the relevant spectrum was failed to acquire for **43** due to the insufficient abundance. After referring to the compound library[26,35−37], **32**, **36**, and **43** (Supporting Information Fig. S13) were configured as notoginsenoside R4 (*i.e.,* 20-*O*-Xyl-(1→6)-Glc-(1→6)-Glc-[3-*O*-Glc-(1→2)-Glc]-protopanaxadiol), notoginsenoside Fa (*i.e.,* 20-*O*-Glc-(1→6)-Glc-[3-*O*-Xyl-(1→2)-Glc-(1→2)-Glc]-protopanaxadiol), and ginsenoside Ra3 (*i.e.,* 20-*O*-Xyl-(1→3)-Glc-(1→6)-Glc-[3-*O*-Glc-(1→2)-Glc]-protopanaxadiol), respectively. Fortunately, these compounds were successfully collected from the market, and as expected, LC−MS/MS behaviors of **32**, **36**, and **43** were exactly consistent to those of authentic ginsenosides.

Using the "top-down" structural annotation strategy, confidence-enhanced identities were also assigned to the other differential variables such as **35** (notoginsenoside T/notoginsenoside D), **42** (chikusetusaponin L5), **47** (notoginsenoside R2), **49** (notoginsenoside Fc), and **78** (vinaginsenoside R17/vinaginsenoside R18). Notably, Rb3 (**60**) and Rc (**50**), and F2 (**17**) should be unique for the aerial and underground parts of ginseng, respectively, while Rb1 (**45**) played the key role to differentiating roots from rhizomes.

Because of integrating full concentration ramp-MS^1, FCER-MS^2, and FEER-MS^3 spectra, 3×3D-MS/MS spectrum comprehensively covers temporal MS/MS behaviors of a given compound. Its relationships with concentration and structure significantly facilitate quantitative settings optimization, and more importantly, confirmative structure identification. Due to involving all information in the routine spectra, the existing MS/MS knowledge including the well-defined mass cracking laws and those versatile databases (*e.g.*, HMDB, Metlin, ChemSpider, and MassBank) is completely applicable for 3×3D-MS/MS concept. Additionally, 1st 3D spectrum provides auxiliary structural evidences in addition to molecular formula, and reveals that the signal diversity, to some extent, leads to the limited dynamic range when employing MS^1 signal response for quantitative analysis. The 2nd 3D spectrum is advantageous at providing linkage information amongst different substructures, notably when being aided by quantum structure calculation[19]. Moreover, it provides a meaningful opportunity to build the correlations between OCEs and certain masses, resulting in an efficient strategy for MRM parameters optimization in an authentic compound-independent

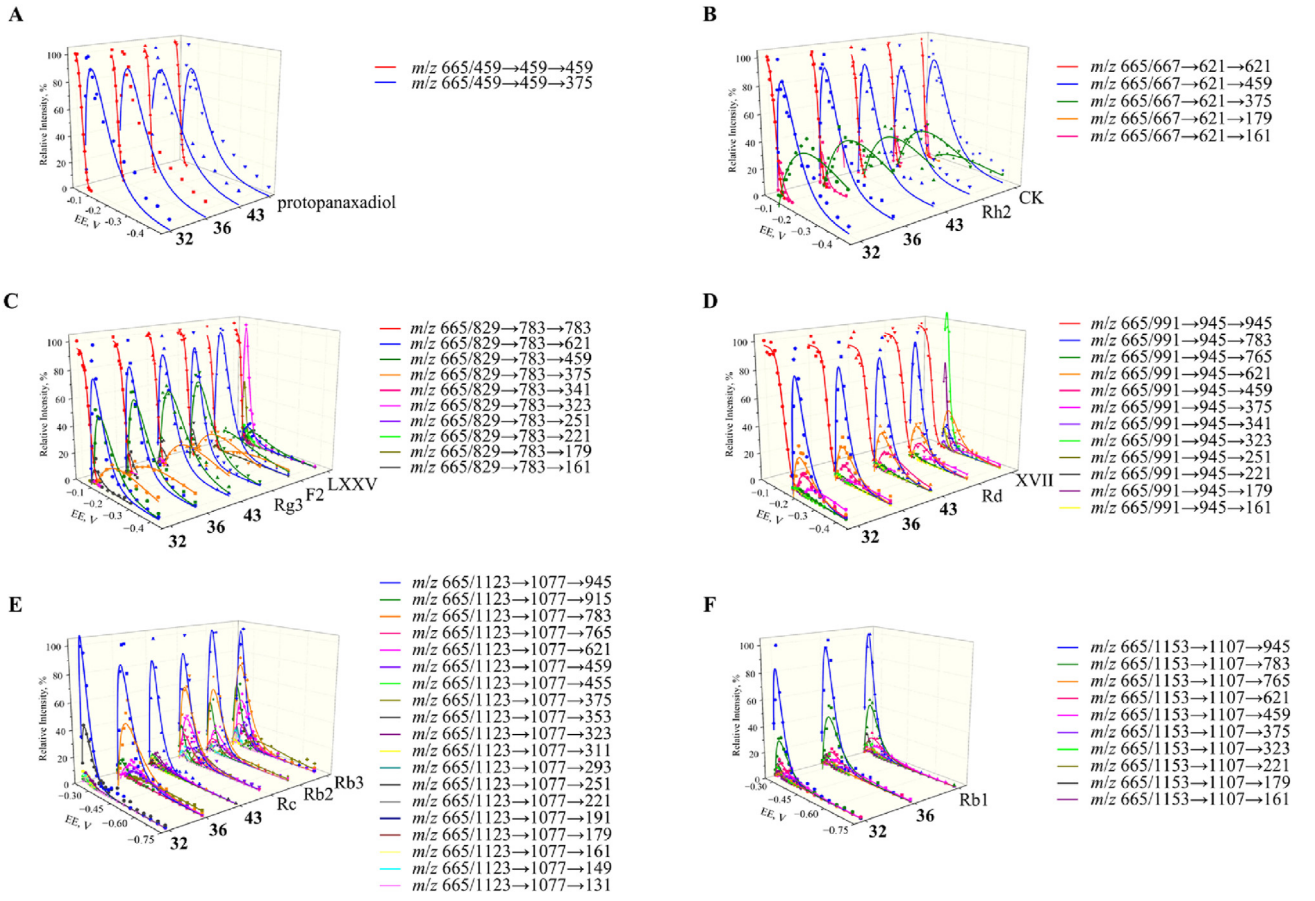

Figure 7 FEER-MS^n spectra (n = 3 for compounds **32**, **36**, and **43**, and n = 2 for the other compounds) comparison among the concerned fragment ions of **32**, **36**, and **43** and anions of suspected decomposition products. FEER-MS^n spectra of *m/z* 459.4 (A) for **32**, **36**, and **43**, as well as protopanoxadiol, FEER-MS^n spectra of *m/z* 621.4 (B) for **32**, **36**, and **43**, as well as Rh2 and CK, FEER-MS^n spectra of *m/z* 783.5 (C) for **32**, **36**, and **43**, as well as Rg3, F2, and LXXV, FEER-MS^n spectra of *m/z* 945.5 (D) for **32**, **36**, and **43**, as well as Rd and XVII, FEER-MS^n spectra of *m/z* 1077.6 (E) for **32**, **36**, and **43**, as well as Rc, Rb2, and Rb3, and FEER-MS^n spectra of *m/z* 1107.6 (F) for **32**, **36**, and **43**, as well as Rb1.

manner. Owing to focusing on the dissociation trajectories from 1st- to 2nd-generation fragment ions, 3rd 3D spectrum implies fruitful information for the substructures[20], and such clues can also be decoded to certain MDs through quantum structure calculation. More importantly, matching FEER-MS^3 with FEER-MS^2 of the empirical decomposition product dramatically benefits the "top-down" structural identification strategy.

Indeed, it is quite tedious to construct the entire 3×3D-MS/MS spectrum and the incorporation of HR-MS/MS (*e.g.*, QTOF-MS, IT-TOF-MS, and Obitrap-MS) and Qtrap-MS is favored. In practice, merely a portion of information is mandatory to advance quantitative sub-metabolomics. Fortunately, either each 3D spectrum or the relevant relationships are stand-alone, and it is convenient to choose the fit-for-purpose building block(s). Both MS^2 and MS^3 spectra, theoretically, are the sections at the sole CE and EE levels of FCER-MS^2 and FEER-MS^3 spectra, accordingly, and they also carry wealthy information, such as masses and relative ion abundances. Under most statuses, those snapshots are able to replace the roles of FCER-MS^2 and FEER-MS^3. For instance, through employing appropriate EE settings, MS^3 and MS^2 spectral comparison is feasible to determine whether the substructure is identical with the decomposition product structure. Due to the mild structural difference, it is still challenging to discriminate C-20 configurational isomers using 3×3D-MS/MS spectrum. To address this obstacle, it might be viable to employ strategies such as metal complex configuration[14] and quantitative structure−retention relationship modeling[39].

After re-analyzing MS^1 spectra accumulated in our group[19,20,28,40,41], singly charged multimer anions/cations are ubiquitously detected for diverse chemical families; however, the multi-charged multimer anions solely occur for saponins possessing more than two sugar chains. To preliminarily clarify this phenomenon, a post-column infusion assay was conducted through individually fortifying pure ginsenosides with a T-piece[42] when measuring the mixed standard sample (Supporting Information Fig. S14). MS^1 spectra for the co-elution of F2 & Rg1/Rf/F11, Rg3 & Rg1/Rf/F11, and LXXV & Rg1/Rf/F11, representatively, are depicted in Supporting Information Fig. S15. The singly charged hetero-multimer anion was observed for all cases, whilst doubly charged heterodimer anions at *m/z* 837.49 ($[M_1+M_2+2HCOO]^{2-}$) were observed merely for F2 & Rg1/Rf, and Rg3 & Rg1. Obviously, doubly charged complexes of heterodimer (*i.e.*, $[M_1+M_2+2HCOO]^{2-}$), as well as some other multi-charged heteromeric anions, could be observed when the co-elution of bidesmosidic ginsenosides, whilst the singly charged multimer anions, *e.g.*, $[M_1+M_2+HCOO]^-$, were observed for any

co-elution. Moreover, $[M_1+M_2+2HCOO]^{2-}$ ions appeared at even extremely low concentrations for co-eluted bidesmosidic ginsenosides, and this ion species was totally absent for two monodesmosidic ginsenosides at high contents. Consequently, we deduced that the ability of at least one saponin to be doubly charged is the prerequisite for the existence of multiply charged complexes for heterodimers or homodimers. Two separate sugar chains are individually charged by ESI source[43], resulting in the occurrences of multi-charged multimer anions. Noteworthily, because the peak capacity of a given column usually could not meet the chromatographic separation requirements of notoginseng materials, special attention should be paid onto such heteromeric anions when the co-elution occurs[31].

Compared to several well-organized studies[35,36,44], less ginsenosides were characterized in notoginseng. Attributing to the great efforts made by the scientists worldwide, it isn't challenging now to capture hundreds of ginsenosides through employing either sensitive data acquisition methods or robust post-acquisition data processing strategies[45]. The bottlenecks for in-depth sub-metabolome clarification, actually, locate at confidence-strengthened identification and globally quantitative analysis. Exactly, this study primarily focused on advancing the qualitative and quantitative performances of MS/MS, and the findings demonstrated 3×3D-MS/MS spectrum concept could benefit the technical barrier breakthroughs. Moreover, the combination of the new concept with the conventional strategies should give a birth to more robust analytical tool for quantitative metabolomics.

4. Conclusions

To propel MS/MS being eligible for sub-metabolomics, 3×3D-MS/MS concept was proposed to universally involve MS/MS behaviors of a given compound *via* applying concentration-resolved program to MS^1 recording and ER-MS program to either MS^2 or MS^3 acquisition. 3×3D-MS/MS spectrum was configured by full concentration ramp-MS^1, FCER-MS^2, and FEER-MS^3, corresponding to 1st, 2nd, and 3rd 3D spectra, accordingly. Quantitative characterization of ginsenosides-targeted sub-metabolome in notoginseng was employed as a proof-of-concept. The correlations between 3×3D-MS/MS and structural/concentration features were constructed by assaying a set of authentic ginsenosides. Bidesmosidic saponins produced fruitful multicharged multimer anions (*e.g.*, $[2M-2H]^{2-}$ and $[2M+2HCOO]^{2-}$), resulting in a unique $ISR_{0.5:0}$ feature, and moreover, $ISR_{1:0}$ was significantly lower than monodesmosidic isomers. FCER-MS^2 and FEER-MS^3 involved all the trajectories for the dissociations from quasi-molecular ion to 1st-generation fragment ions and from the selected 1st-generation fragment ion to 2nd-generation fragment ions, respectively. OCEs for 1st-generation fragment ions were roughly, linearly correlated with the masses of precursor and fragment ions, leading to a superior approach for quantitative MRM program development. OCE was also partially governed by the glycosidation site. More importantly, FEER-MS^3 spectrum of certain 1st-generation fragment ion for a given ginsenoside was exactly identical with FEER-MS^2 spectrum of the anion for the hydrolysis product when they shared the same molecular geometries. Through applying the relationships, quantitative sub-metabolome characterization succeeded through identifying and quantifying 95 ginsenosides, and significant differences occurred amongst different parts of notoginseng. Noteworthily, the differential saponins were unequivocally identified *via* applying "top-down" strategy where the structures of those progressive 1st-generation fragment ions were deciphered by matching with the step-wise hydrolysis products for the concerned ginsenoside. Above all, 3×3D-MS/MS significantly boosts both qualitative and quantitative potentials of MS/MS without updating any hardware, because it comprehensively covers MS/MS behaviors of a given compound.

Acknowledgments

This study were financially supported by the National Natural Science Foundation of China (No. 81973444) and National Administration of Traditional Chinese Medicine High level Key Discipline Construction Project of Traditional Chinese Medicine—Chemistry of Chinese Materia Medica.

Author contributions

Ke Zhang: Investigation, Methodology, Writing − original draft. Jinru Jia: Conceptualization, Writing − original draft. Ting Li: Data curation, Visualization. Wenjing Liu: Investigation, Methodology. Pengfei Tu: Conceptualization, Project administration, Supervision. Jian-Bo Wan: Conceptualization, Project administration, Supervision. Jun Li: Conceptualization, Project administration, Supervision. Yuelin Song: Conceptualization, Funding acquisition, Writing − review & editing.

Conflicts of interest

The authors declare no conflicts of interest.

Appendix A. Supporting information

Supporting information to this article can be found online at https://doi.org/10.1016/j.apsb.2024.04.029.

References

1. An N, Zhu QF, Wang YZ, Xiong CF, Hu YN, Feng YQ. Integration of chemical derivatization and in-source fragmentation mass spectrometry for high-coverage profiling of submetabolomes. *Anal Chem* 2021;**93**:11321−8.
2. Zhao S, Li H, Han W, Chan W, Li L. Metabolomic coverage of chemical-group-submetabolome analysis: group classification and four-channel chemical isotope labeling LC−MS. *Anal Chem* 2019;**91**:12108−15.
3. Yuan BF, Zhu QF, Guo N, Zheng SJ, Wang YL, Wang J, et al. Comprehensive profiling of fecal metabolome of mice by integrated chemical isotope labeling-mass spectrometry analysis. *Anal Chem* 2018;**90**:3512−20.
4. Calderón-Santiago M, Priego-Capote F, Luque De Castro MD. Enhanced detection and identification in metabolomics by use of LC−MS/MS untargeted analysis in combination with gas-phase fractionation. *Anal Chem* 2014;**86**:7558−65.
5. Chen J, Zhang P, Qin S, Tan B, Li S, Tang S, et al. Stepwise solid phase extraction integrated with chemical derivatization for all-in-one injection LC−MS/MS analysis of metabolome and lipidome. *Anal Chim Acta* 2023;**1241**:340807.
6. Vasilopoulou CG, Sulek K, Brunner AD, Meitei NS, Schweiger-Hufnagel U, Meyer SW, et al. Trapped ion mobility spectrometry and PASEF enable in-depth lipidomics from minimal sample amounts. *Nat Commun* 2020;**11**:331.

7. Zha H, Cai Y, Yin Y, Wang Z, Li K, Zhu ZJ. SWATHtoMRM: development of high-coverage targeted metabolomics method using SWATH technology for biomarker discovery. *Anal Chem* 2018;**90**: 4062−70.
8. Wang CF, Li L. Instrument-type effects on chemical isotope labeling LC−MS metabolome analysis: quadrupole time-of-flight MS *vs*. Orbitrap MS. *Anal Chim Acta* 2022;**1226**:340255.
9. Wishart DS, Guo A, Oler E, Wang F, Anjum A, Peters H, et al. HMDB 5.0: the human metabolome database for 2022. *Nucleic Acids Res* 2022;**50**:D622−31.
10. Guijas C, Montenegro-Burke JR, Domingo-Almenara X, Palermo A, Warth B, Hermann G, et al. METLIN: a technology platform for identifying knowns and unknowns. *Anal Chem* 2018;**90**:3156−64.
11. Little JL, Williams AJ, Pshenichnov A, Tkachenko V. Identification of "known unknowns" utilizing accurate mass data and chemspider. *J Am Soc Mass Spectrom* 2012;**23**:179−85.
12. Shi C, Jia H, Chen S, Huang J, Peng Y, Guo W. Hydrogen/deuterium exchange aiding metabolite identification in single-cell nanospray high-resolution mass spectrometry analysis. *Anal Chem* 2022;**94**: 650−7.
13. Horai H, Arita M, Kanaya S, Nihei Y, Ikeda T, Suwa K, et al. MassBank: a public repository for sharing mass spectral data for life sciences. *J Mass Spectrom* 2010;**45**:703−14.
14. Song Y, Song Q, Liu W, Li J, Tu P. High-confidence structural identification of metabolites relying on tandem mass spectrometry through isomeric identification: a tutorial. *TrAC Trend Anal Chem* 2023;**160**: 116982.
15. Zhang JY, Zhang Q, Li N, Wang ZJ, Lu JQ, Qiao YJ. Diagnostic fragment-ion-based and extension strategy coupled to DFIs intensity analysis for identification of chlorogenic acids isomers in Flos Lonicerae Japonicae by HPLC−ESI-MS^n. *Talanta* 2013;**104**: 1−9.
16. Yuan H, Chen F, Zhang M, Ma S, Qu M, Zhao W, et al. Rapid identification and relative quantification of disaccharide isomers by three fragment ion pairs using ESI-MS/MS and its application in yellow rice wine. *Food Chem* 2023;**409**:135340.
17. Xiu Y, Ma L, Zhao H, Sun X, Li X, Liu S. Differentiation and identification of ginsenoside structural isomers by two-dimensional mass spectrometry combined with statistical analysis. *J Ginseng Res* 2019; **43**:368−76.
18. Hernandez J, Müller A, Jaiswal R, Davalos JZ, Kuhnert N. Energy resolved mass spectrometry of chlorogenic acids and its application to isomer quantification by direct infusion tandem mass spectrometry. *Phytochem Anal* 2018;**29**:406−12.
19. Guan P, Liu W, Cao Y, Tang H, Huo H, Wan JB, et al. Full collision energy ramp-MS^2 spectrum in structural analysis relying on MS/MS. *Anal Chem* 2021;**93**:15381−9.
20. Cao Y, Li W, Chen W, Niu X, Wu N, Wang Y, et al. Squared energy-resolved mass spectrometry advances quantitative bile acid submetabolome characterization. *Anal Chem* 2022;**94**: 15395−404.
21. Zhao N, Cheng M, Huang S, Liu D, Zhao Q, Bai Y, et al. Various multicharged anions of ginsenosides in negative electrospray ionization with QTOF high-resolution mass spectrometry. *J Am Soc Mass Spectrom* 2019;**30**:403−18.
22. Zhao M, Linghu KG, Xiao L, Hua T, Zhao G, Chen Q, et al. Anti-inflammatory/anti-oxidant properties and the UPLC−QTOF/MS-based metabolomics discrimination of three yellow camellia species. *Food Res Int* 2022;**160**:111628.
23. Peris-Díaz MD, Rodak O, Sweeney SR, Krężel A, Sentandreu E. Chemometrics-assisted optimization of liquid chromatography−quadrupole-time-of-flight mass spectrometry analysis for targeted metabolomics. *Talanta* 2019;**199**:380−7.
24. Zheng F, Zhao X, Zeng Z, Wang L, Lv W, Wang Q, et al. Development of a plasma pseudotargeted metabolomics method based on ultra-high-performance liquid chromatography−mass spectrometry. *Nat Protoc* 2020;**15**:2519−37.
25. Song Y, Song Q, Liu Y, Li J, Wan JB, Wang Y, et al. Integrated workflow for quantitative metabolome profiling of plants, Peucedani Radix as a case. *Anal Chim Acta* 2017;**953**:40−7.
26. Li X, Liu J, Zuo T, Hu Y, Li Z, Wang H, et al. Advances and challenges in ginseng research from 2011 to 2020: the phytochemistry, quality control, metabolism, and biosynthesis. *Nat Prod Rep* 2022;**39**: 875−909.
27. Jung SC, Kim W, Park SC, Jeong J, Park MK, Lim S, et al. Two ginseng UDP-glycosyltransferases synthesize ginsenoside Rg3 and Rd. *Plant Cell Physiol* 2014;**55**:2177−88.
28. Zhang K, Liu W, Song Q, Wan JB, Yu J, Gong X, et al. Integrated strategy drives direct infusion−tandem mass spectrometry as an eligible tool for shotgun pseudo-targeted metabolomics of medicinal plants. *Anal Chem* 2021;**93**:2541−50.
29. Gross JH. *Mass spectrometry. A textbook*. 3rd ed. Springer Science & Business Media; 2017. p. 89.
30. Feith A, Teleki A, Graf M, Favilli L, Takors R. HILIC-Enabled ^{13}C metabolomics strategies: comparing quantitative precision and spectral accuracy of QTOF high- and QQQ low-resolution mass spectrometry. *Metabolites* 2019;**9**:63.
31. Jia J, Zhang K, Wang S, Yu J, Li J, Tu P, et al. Hybrid complex anions of ginsenosides resulted from direct infusion−tandem mass spectrometry. *Rapid Comm Mass Spectrom* 2022;**36**:e9319.
32. Liu W, Li W, Zhang P, Gong X, Tu P, Tang L, et al. Quality structural annotation for the metabolites of chlorogenic acid in rat. *Food Chem* 2022;**379**:132134.
33. Kertesz TM, Hall LH, Hill DW, Grant DF. CE_{50}: quantifying collision induced dissociation energy for small molecule characterization and identification. *J Am Soc Mass Spectrom* 2009;**20**:1759−67.
34. Chait BT. Mass spectrometry: bottom-up or top-down?. *Science* 2006; **314**:65−6.
35. Jia L, Wang H, Xu X, Wang H, Li X, Hu Y, et al. An off-line three-dimensional liquid chromatography/Q-Orbitrap mass spectrometry approach enabling the discovery of 1561 potentially unknown ginsenosides from the flower buds of *Panax ginseng, Panax quinquefolius* and *Panax notoginseng*. *J Chromatogr A* 2022;**1675**:463177.
36. Yang W, Ye M, Qiao X, Liu C, Miao W, Bo T, et al. A strategy for efficient discovery of new natural compounds by integrating orthogonal column chromatography and liquid chromatography/mass spectrometry analysis: its application in *Panax ginseng, Panax quinquefolium* and *Panax notoginseng* to characterize 437 potential new ginsenosides. *Anal Chim Acta* 2012; **739**:56−66.
37. Yang W, Hu Y, Wu W, Ye M, Guo D. Saponins in the genus *Panax* L. (Araliaceae): a systematic review of their chemical diversity. *Phytochemistry* 2014;**106**:7−24.
38. Shi X, Yang W, Qiu S, Yao C, Shen Y, Pan H, et al. An in-source multiple collision-neutral loss filtering based nontargeted metabolomics approach for the comprehensive analysis of malonylginsenosides from *Panax ginseng*, *P. quinquefolius*, and *P. notoginseng*. *Anal Chim Acta* 2017;**952**:59−70.
39. Haddad PR, Taraji M, Szücs R. Prediction of analyte retention time in liquid chromatography. *Anal Chem* 2021;**93**:228−56.
40. Xu X, Li W, Li T, Zhang K, Song Q, Liu L, et al. Direct infusion-three-dimensional-mass spectrometry enables rapid chemome comparison among herbal medicines. *Anal Chem* 2020;**92**: 7646−56.
41. Song Q, Li J, Huo H, Cao Y, Wang Y, Song Y, et al. Retention time and optimal collision energy advance structural annotation relied on LC−MS/MS: an application in metabolite identification of an antidementia agent namely echinacoside. *Anal Chem* 2019;**91**: 15040−8.

42. Moser C, Zoderer D, Luef G, Rauchenzauner M, Wildt L, Griesmacher A, et al. Simultaneous online SPE-LC−MS/MS quantification of six widely used synthetic progestins in human plasma. *Anal Bioanal Chem* 2012;**403**:961−72.
43. Yan Z, Lin G, Ye Y, Wang Y, Yan R. Triterpenoid saponins profiling by adducts-targeted neutral loss triggered enhanced resolution and product ion scanning using triple quadrupole linear ion trap mass spectrometry. *Anal Chim Acta* 2014;**819**:56−64.
44. Yao C, Pan H, Wang H, Yao S, Yang W, Hou J, et al. Global profiling combined with predicted metabolites screening for discovery of natural compounds: characterization of ginsenosides in the leaves of *Panax notoginseng* as a case study. *J Chromatogr A* 2018;**1538**:34−44.
45. Yu Y, Yao C, Guo D. Insight into chemical basis of traditional Chinese medicine based on the state-of-the-art techniques of liquid chromatography−mass spectrometry. *Acta Pharm Sin B* 2021;**11**:1469−92.